



Cite this: DOI: 10.1039/d5sm00116a

Characterizing semiflexible network structure of wormlike micelles by dynamic techniques†

 Hiroki Degaki,^a Tsuyoshi Koga^a and Tetsuharu Narita^{a,b*}

Understanding the structure–property relationships of semiflexible polymer networks is essential for their rational design and application across diverse fields. While classical static structural characterizations have been widely used, dynamic investigations also provide a powerful approach to analyzing these networks across multiple hierarchical levels in both time and length scales. This study presents a comprehensive methodology to dynamically determine key structural parameters in semiflexible polymer networks, characterizing time, length, volume, and molecular weight of unit segments at their respective hierarchical levels, such as Kuhn monomers, correlation blobs, and network strands. A wormlike micellar solution of sodium dodecyl sulfate and aluminum nitrate was used as a model system representing semiflexible polymers with a large Kuhn length. By combining dynamic experimental techniques, including dynamic light scattering, macrorheology, and microrheology, crucial structural information was obtained. Integrating information derived from the characteristic parameters successfully revealed the hierarchical network structure of the wormlike micelles, with results validated against static light scattering measurements. Notably, this study effectively utilizes the complex viscoelastic modulus obtained through microrheology, which has received limited attention in the literature. This approach holds potential applicability to a wide range of semiflexible polymer networks.

 Received 3rd February 2025,
 Accepted 1st April 2025

DOI: 10.1039/d5sm00116a

rsc.li/soft-matter-journal

1 Introduction

Polymer chains exhibit rigidity or flexibility depending on the observation length scale. The persistence length (half of the Kuhn length) defines the scale below which a chain behaves as rigid. Chains with persistence lengths comparable to or exceeding typical observation scales, often tens of nanometers or more due to their thick or rigid structures, are classified as semiflexible. In contrast, chains with persistence lengths comparable to their monomer size (or diameter) typically below 1 nm are considered flexible.^{1,2}

In networks formed by semiflexible chains, the persistence length can be comparable to the size of the mesh (the size of the network strand between entanglement points), distinguishing them as a class of polymeric systems different from flexible polymer networks. Notable examples include biopolymers, such as cytoskeletal polymers (*e.g.*, actin filaments,

microtubules and intermediate filaments), whose cross-linked networks with large persistence lengths play crucial roles in the mechanics of tissues and living cells.^{2,3} Wormlike micellar networks, formed by surfactant molecules with small head groups and long tails that preferentially self-assemble into elongated rather than spherical structures, represent another class of systems with large persistence lengths.⁴ Given their abundance in nature^{2,3} and extensive industrial applications,⁴ experimental investigations into the structure–property relationships of semiflexible networks are essential for understanding their behaviors.

Under semidilute or concentrated conditions, polymer network structures can be described hierarchically through unit segments of different size scales: Kuhn monomers, correlation blobs, and meshes (or strands) of the network, in increasing order of size.^{1,5} Within a Kuhn monomer, the chain exhibits bending, a small but significant thermal fluctuation around a straight chain conformation. Correlation blobs are space-filling unit segments composed of Kuhn monomers and solvent, representing the scale at which Kuhn monomers can no longer distinguish between those from the same chain and those from others. Thus, the configuration of a partial chain within a mesh, formed by entanglements or crosslinks and composed of correlation blobs, can be modelled as a random walk of these blobs.

Structures of polymer networks are commonly characterized by scattering techniques. By measuring the scattered intensity

^a Department of Polymer Chemistry, Graduate School of Engineering, Kyoto University, Katsura, Kyoto 615-8510, Japan

^b Laboratoire Sciences et Ingénierie de la Matière Molle, CNRS UMR 7615, ESPCI Paris, Sorbonne Université, PSL Université, 75005 Paris, France.

E-mail: tetsuharu.narita@espci.fr

† Electronic supplementary information (ESI) available: Determination of overlap concentration, details of DLS results, moduli obtained by macrorheology and microrheology, comparison between macrorheology and microrheology, and Zimm plots. See DOI: <https://doi.org/10.1039/d5sm00116a>

of radiation as a function of the scattering vector q , power-law behaviors corresponding to different chain configurations can be observed. Adjusting the scattering angle as well as the radiation wavelength from visible light to X-rays allows probing a wide range of length scales. Key structural parameters, such as characteristic length (e.g., Kuhn length, correlation length, and radius of wormlike micelles) and molecular weight, can be obtained through these scattering techniques.^{1,6–8}

Dynamic properties of polymer networks are also important as they reflect the underlying structures. Dynamic light scattering (DLS) is a primary method for probing network dynamics, enabling detection of diffusive motions associated with the correlation length through time-dependent fluctuations in scattered light.¹ Classical rheometry, or macrorheology, has been used to estimate the molecular weight of network strands using the elastic plateau modulus.^{9,10} While macrorheology is limited in its accessible frequency range and cannot capture the fast characteristic relaxation of small unit segments, microrheology extends the capability to the high-frequency regime.¹¹ It has been successfully applied to determine the Kuhn length, the characteristic length of the smallest structural units.^{11–14}

In this study, we characterize the hierarchical structure of semiflexible polymer networks across multiple length scales by integrating various dynamic methods: DLS, macrorheology, and microrheology based on diffusing-wave spectroscopy (DWS) and DLS. Key structural parameters of wormlike micellar semiflexible chains, including relaxation times, characteristic lengths, volumes, and molecular weights of unit segments, are experimentally evaluated and compared with static light scattering (SLS) results. Notably, we use absolute values of the complex viscoelastic moduli obtained from macro- and microrheometry, an aspect that has received limited attention in prior studies.¹⁵

As a representative system of semiflexible polymers, we investigate a wormlike micellar solution of sodium dodecyl sulfate (SDS), a widely used anionic surfactant, and aluminum nitrate ($\text{Al}(\text{NO}_3)_3$). This system is notable for its application in the synthesis of mesoporous alumina particles^{16–20} and as an example of wormlike micelles with a large persistence length, which has yet to be fully examined dynamically.

2 Experimental

2.1 Materials

SDS and aluminum nitrate nonahydrate ($\text{Al}(\text{NO}_3)_3 \cdot 9\text{H}_2\text{O}$) were purchased from Sigma-Aldrich. An aqueous suspension of polystyrene microspheres (particle size: 500 nm, plain surface) used as probe particles for microrheology experiments based on DWS and DLS was obtained from Micromod (Rostock, Germany). All the chemicals were used as received without further purification.

2.2 Sample preparation

SDS/ $\text{Al}(\text{NO}_3)_3$ aqueous solutions at varied SDS concentrations and at a constant $\text{Al}(\text{NO}_3)_3 \cdot 9\text{H}_2\text{O}$ concentration (1 mol L⁻¹) were

prepared by mixing SDS and $\text{Al}(\text{NO}_3)_3 \cdot 9\text{H}_2\text{O}$ in Milli-Q water at room temperature. For single scattering measurements (SLS, DLS, and DLS microrheology), Milli-Q water filtered with a 0.2 μm syringe filter was used, and the final SDS/ $\text{Al}(\text{NO}_3)_3$ solutions were filtered with 0.8 μm syringe filters. For DWS and DLS microrheology measurements, the aqueous suspension of the probe particles was added to the SDS/ $\text{Al}(\text{NO}_3)_3$ solution. The probe concentration was set to 1 wt% for DWS and 0.001 wt% for DLS microrheology.

2.3 DWS microrheology

DWS microrheology measurements²¹ were performed using a laboratory-made setup. The coherent light source was a spectrophysics excelsior laser (wavelength: 532 nm, output power: 300 mW). The laser beam was expanded to approximately 1 cm in diameter at samples. Samples were prepared in plastic cuvettes for spectroscopy with a path length $L = 4$ nm and placed in a thermostated sample holder at 25 °C. The scattered light was collected by an optical fiber placed in the transmission geometry, connected to a photon counter to obtain the intensity autocorrelation function. A digital correlator (ALV-7004/USB-FAST, ALV, Langens, Germany) was used to treat signals.

The obtained intensity autocorrelation function $g^{(2)}(t)$ was converted into the field autocorrelation function $g^{(1)}(t)$ using the Siegert relation $g^{(2)}(t) = 1 + \beta[g^{(1)}(t)]^2$ (β is an instrumental factor). Then, the mean square displacement of a probe particle, $\langle \Delta r^2(t) \rangle$, was calculated by numerically solving the following equations for transmission geometry:²²

$$g^{(1)}(t) = \frac{L}{l^*} + \frac{4}{3} \frac{z_0}{l^*} + \frac{2}{3} \frac{\sinh\left[\frac{z_0}{l^*}\tilde{r}(t)\right] + \frac{2}{3}\tilde{r}(t)\cosh\left[\frac{z_0}{l^*}\tilde{r}(t)\right]}{\left(1 + \frac{4}{9}\tilde{r}(t)^2\right)\sinh\left[\frac{L}{l^*}\tilde{r}(t)\right] + \frac{4}{3}\tilde{r}(t)\cosh\left[\frac{L}{l^*}\tilde{r}(t)\right]} \quad (1)$$

where $\tilde{r}(t) \equiv \sqrt{(2\pi/\lambda)^2 \langle \Delta r^2(t) \rangle}$ is the root of the mean square displacement nondimensionalized by the wavelength λ , and l^* is the sample transport mean free path of the scattered light. The value of l^* was determined from the transmission intensity of the sample and that of water, whose l^* value in the literature is 210 μm .²³ For the wormlike micellar solutions studied in this work, we found $l^* = 340 \pm 11$ μm . The distance that the light must travel through the sample before becoming randomized, z_0 , was here set to $z_0 = l^*$. The frequency dependence of the dynamic modulus was estimated using the generalized Stokes-Einstein equation:

$$G^*(\omega) = \frac{k_B T}{\pi R i \omega \langle \Delta \tilde{r}^2(\omega) \rangle} \quad (2)$$

where k_B is the Boltzmann constant, T is temperature, R is the radius of the probe particle, and $\langle \Delta \tilde{r}^2(\omega) \rangle$ is the Laplace transform of $\langle \Delta r^2(t) \rangle$, which is approximated as $i\omega \langle \Delta \tilde{r}^2(\omega) \rangle \simeq [\langle \Delta r^2(t) \rangle \Gamma(1 + \partial \ln \langle \Delta r^2(t) \rangle / \partial \ln t)]_{t=1/i\omega}$.²⁴

2.4 DLS and SLS (without probe particles)

Dynamic and static light scattering measurements were performed with an ALV CGS-3 goniometer system (ALV, Langen, Germany) equipped with a He-Ne laser (22 mW at $\lambda = 632.8$ nm) at 25 °C. The filtered SDS/Al(NO₃)₃ solutions were prepared in test tubes (diameter: 10 mm). For DLS, the system measured the time-averaged autocorrelation function of the scattered light intensity at a scattering vector defined as $q = 4\pi n/\lambda \sin(\theta/2)$, where n is the refractive index of the solution, and θ is the scattering angle. For SLS, the scattered light intensity over the duration of the measurement was recorded. The scattering angle was varied between 30 and 150°. The reference value 0.1 mL g⁻¹ of refractive index increment was used for Zimm plots.²⁵

2.5 DLS microrheology (with probe particles)

DLS microrheology measurements²⁶ were performed with the same apparatus as the DLS measurements described above, for SDS/Al(NO₃)₃ solutions with probe particles. The concentration of the probe particles was fixed to 0.001 wt%, which was considered to be high enough to obtain a much higher scattered intensity in comparison with the scattered intensity coming from the micelles but low enough to avoid multiple scattering. This concentration of microparticles was experimentally determined considering the relation of the scattered intensity for microparticle aqueous dispersion (I_{up}) and aqueous solution of SDS for a concentration of 4 wt% (I_{SDS}), obtaining a value $I_{\text{up}}/I_{\text{SDS}} = 30$ for the chosen concentration of microparticles.

As for DWS, the obtained intensity autocorrelation function $g^{(2)}(t)$ was converted into the field autocorrelation function $g^{(1)}(t)$ by the Siegert relation. The mean square displacement $\langle \Delta r^2(t) \rangle$ was then calculated by the following equation:

$$g^{(1)}(q, t) = \exp \left[-\frac{\langle \Delta r^2(t) \rangle \cdot q^2}{6} \right] \quad (3)$$

2.6 Macrorheology

Macroscopic rheological measurements of wormlike micellar solutions were performed with a stress-controlled Kaake RS600 rheometer using cone-plate geometry (diameter: 35 mm, angle: 2°, gap: 103 μm). Frequency sweep (between 0.01 and 100 rad s⁻¹) was performed with fixed amplitude in the linear domain. All the measurements were performed at 25 °C, using a laboratory-made anti-evaporation system.

3 Results and discussion

3.1 DLS

DLS, which has been widely used to study wormlike micellar systems in semidilute conditions,^{27–29} is applied to the system investigated in this study. The value of the overlap concentration C_{SDS}^* was determined to be 0.15 wt% from a peak of the static correlation length measured by static light scattering

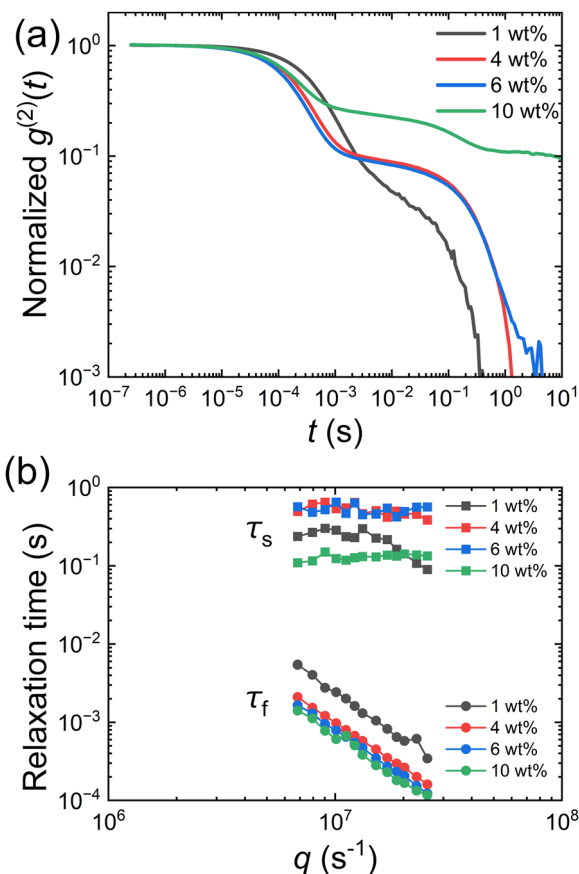


Fig. 1 (a) Normalized intensity autocorrelation function $g^{(2)}(t)$ of SDS/Al(NO₃)₃ aqueous solutions at different SDS concentrations. Scattering angle: 90°. (b) Relaxation times τ_f and τ_s as functions of q .

(Fig. S1, ESI†).²⁸ The details are given in the ESI.† Fig. 1a shows the normalized intensity autocorrelation function $g^{(2)}(t)$ of SDS/Al(NO₃)₃ aqueous solutions at different SDS concentrations (denoted as C_{SDS} in wt%) within semidilute regime at $\theta = 90^\circ$. The autocorrelation functions exhibit two decorrelation modes: one (fast mode) found between 10^{-4} and 10^{-3} s, and the other (slow mode) above 0.1 s. Similar bimodal autocorrelations were reported for different wormlike micelle systems.^{27–29} As shown in Fig. S2 (ESI†) at 0.1 wt% (concentration below C_{SDS}^*), the autocorrelation function is monomodal. With increase in the concentration, the autocorrelation function becomes bimodal and the amplitude of the appearing slower relaxation mode increases with concentration. At $C_{\text{SDS}} = 10$ wt%, the slow mode does not fully decorrelate, suggesting existence of a further slower mode. In this work we focus on the fast and slow modes.

The relaxation times of these modes were determined by fitting the normalized field autocorrelation with multicomponent stretched exponential function.³⁰ The details of the fit are given in the ESI.† The value of the relaxation times are plotted against the scattering vector q (Fig. 1b). The relaxation time of the fast mode, τ_f , found in the order of 10^{-4} – 10^{-2} s, decreases with increasing q , showing a power-law decay with an exponent of about -2 . This indicates that the fast mode is diffusive, or τ_f corresponds to the time required for the scattering objects to

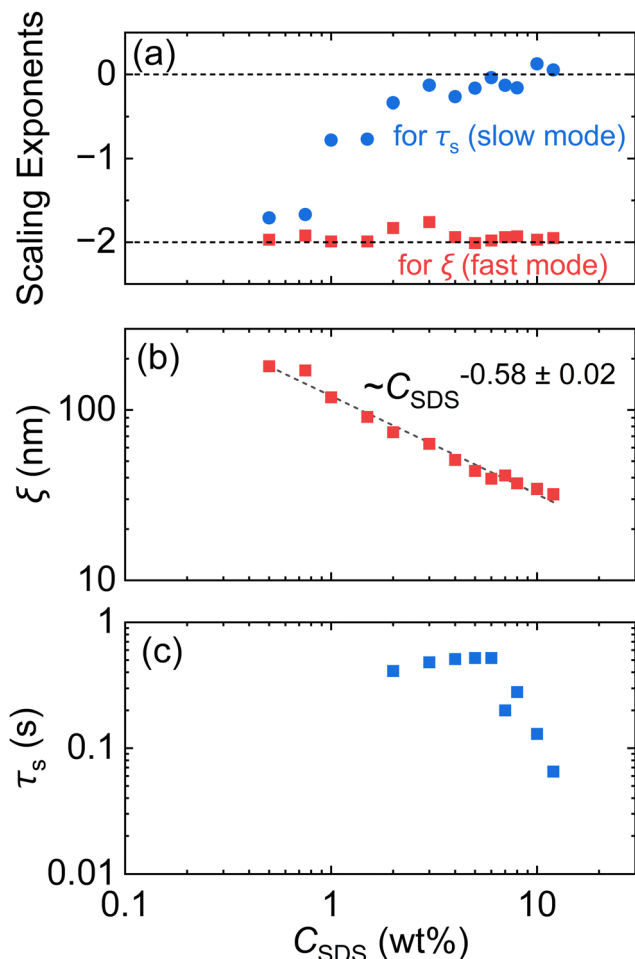


Fig. 2 (a) Power-law exponents for the fast and slow modes as functions of the SDS concentration C_{SDS} . Red squares: fast mode. Blue circles: slow mode. (b) Correlation length ξ and (c) average relaxation time of the slow mode τ_s as functions of C_{SDS} .

diffuse at the length scale of q^{-1} . The relaxation time of the slow mode, τ_s , does not depend on q except 1 wt%. This result indicates that the slow mode does not depend on the observation length scale q , thus corresponds to macroscopic relaxation. The same behavior was reported for other wormlike micellar systems.^{27–29} At $C_{\text{SDS}} = 1$ wt%, the value of τ_s is constant at low q range, while it decreases with increasing q at high q range. While this result suggests the presence of another diffusive mode, we do not further characterize it.

Concentration dependencies of the power-law exponent for the fast and slow modes are investigated, and results are plotted in Fig. 2a. Within the studied SDS concentration range between 0.5 and 12 wt%, the fast mode exhibits the diffusive motion with $\tau_f \propto q^{-2}$. The value of the exponent for the slow mode increases with the SDS concentration to reach 0, and it is between 0 and -2 at the concentrations lower than 2%. The nature of the dynamics is unclear.

Since $\tau_f = 1/Dq^2$ (D is the collective diffusion coefficient), the value of $1/\tau_f$ is plotted against q^2 to determine the value of D from the slope (Fig. S4a, ESI†). By using the Stokes–Einstein

relation, the hydrodynamic size ξ can be determined as

$$\xi = \frac{k_B T}{3\pi\eta D} \quad (4)$$

Within semidilute solutions, the hydrodynamic size is defined as the dynamic correlation length. For the length scales below ξ , the dynamics of chain segments are analogous to those in dilute solutions. Specifically, segments with a size equivalent to ξ exhibit diffusive behavior governed by the solvent viscosity. The value of ξ is plotted as a function of C_{SDS} (Fig. 2b). It decreases with increasing concentration, with a power-law dependence of $\xi \sim C_{\text{SDS}}^{-0.58}$. The exponent 0.58 is smaller than the literature values for wormlike micelles between 0.6 and 0.8, which are associated with the theoretical prediction for flexible polymers in semi-dilute solutions (0.77).^{1,5,31} For highly rigid chains, a smaller exponent of 0.5 is theoretically predicted.³² Consequently, the exponent smaller than the literature values can be possibly attributed to the high chain rigidity in this system. The absolute value of ξ and the chain rigidity will be further discussed in Section 3.3.

For the slow mode, its characteristic time τ_s is found q -independent for $C_{\text{SDS}} \geq 2$ wt%. Thus, the value of τ_s averaged over the q range is plotted as a function of the SDS concentration (Fig. 2c). Up to 6 wt%, the value of τ_s does not strongly depend on the concentration, staying around 0.5 s. A sharp change in the trend is observed between 6 and 7 wt%: τ_s decreases with increasing concentration.

3.2 Macrorheology

Macroscopic relaxation of the SDS/Al(NO₃)₃ solutions was characterized through macrorheological oscillatory shear measurements. In the low-frequency regime, Maxwellian viscoelastic behavior was observed (Fig. S5, ESI†). The terminal relaxation time, zero-shear viscosity, and plateau modulus were determined by fitting with the Maxwell model.

Fig. 3a shows the terminal relaxation time τ_s as a function of the surfactant concentration C_{SDS} . The values are between 0.07 and 0.4 s, peaking at $C_{\text{SDS}} = 6$ wt%. The relaxation time of the slow mode, τ_s , determined by DLS is also plotted. The macroscopic terminal relaxation time and the relaxation time of the slow mode are found to match, except at 4 wt%, indicating that the q -independent slow mode corresponds to the macroscopic relaxation.

The zero-shear viscosity η_0 also exhibits a peak at the same concentration, $C_{\text{SDS}} = 6$ wt% (Fig. 3b). This peak is characteristic of the linear-to-branched transition in wormlike micellar solutions.^{4,33,34} At lower C_{SDS} , linear micelles elongate and become increasingly entangled as C_{SDS} increases, leading to a rise in η_0 and τ_s . In the presence of sufficient counterions (Al³⁺) at a relatively high concentration (1 mol L⁻¹), the anionic charges on the head groups are effectively screened. At higher C_{SDS} , this charge screening facilitates the formation of energetically favorable three- or four-point junctions where the head groups are brought closer together with the reduced number of end caps.⁴ These junctions can slide along the micellar backbone without significant energetic penalty, resulting in

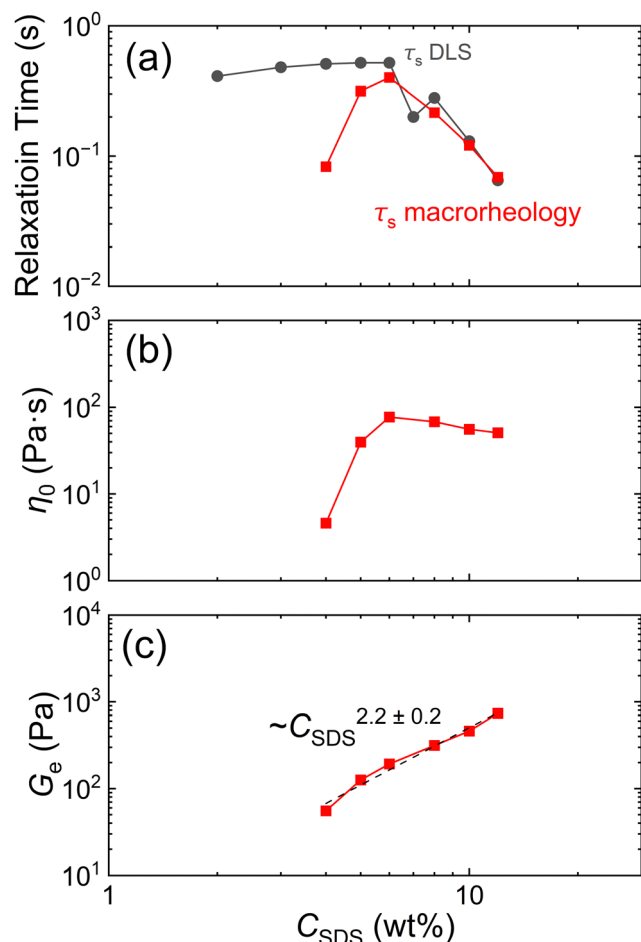


Fig. 3 (a) Macrorheologically measured zero-shear viscosity η_0 . (b) Terminal relaxation time of the slow mode τ_s obtained from macrorheology and DLS measurements without probe particles. (c) Macrorheologically measured plateau modulus G_e .

decrease in η_0 and τ_s .^{4,33} Additionally, the reduced energy barriers enable the transient formation of “ghost-like” crossings, further contributing to the reduction in η_0 and τ_s .⁴

Fig. 3c illustrates the concentration dependence of the plateau modulus, G_e , which increases with C_{SDS} and scales as $G_e \sim C_{\text{SDS}}^{2.2}$. This scaling suggests that both entanglements and branching contribute to G_e , consistent with previous findings.¹³ The scaling exponent of 2.2 aligns with the theoretical prediction of 9/4.³⁵ These macrorheological observations effectively characterize the entangled structures of linear and branched wormlike SDS micelles.

3.3 Microrheology

3.3.1 Comparison between macro- and micro-rheology. To gain deeper insight into finer structural details of the wormlike micelles, microrheological measurements were performed in this study. Classical macrorheology typically covers frequencies up to approximately 10^2 rad s^{-1} , while microrheology, which analyses solutions containing dispersed probe particles using DWS and DLS (distinct from the DLS method for solutions

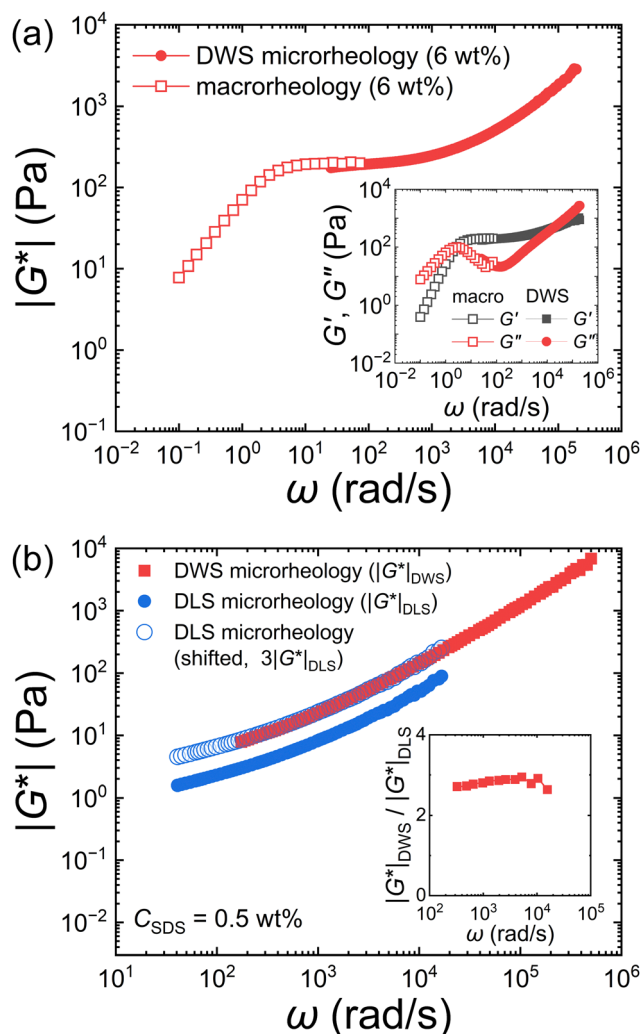


Fig. 4 (a) Polymer contribution to complex modulus (storage and loss moduli in inset) of the SDS 6 wt% solution obtained by oscillatory shear macrorheology and DWS microrheology. (b) Polymer contribution to complex modulus of the SDS 0.5 wt% solution obtained by DWS ($|G^*|_{\text{DWS}}$) and DLS ($|G^*|_{\text{DLS}}$) microrheology. The inset shows the ratio $|G^*|_{\text{DWS}}/|G^*|_{\text{DLS}}$. The open blue circles show shifted $|G^*|_{\text{DLS}}$.

without probe particles described in Section 3.1), extends the accessible frequency range to about 10^5 rad s^{-1} .³⁶ To demonstrate the consistency between these methods, we compared their results. Fig. 4a presents the absolute values of the complex modulus $|G^*|$ and the storage and loss moduli, G' and G'' , measured by DWS microrheology and macrorheology for the 6 wt% SDS solution. In the frequency range between 10 and 10^2 rad s^{-1} , the results from DWS microrheology and macrorheology are reasonably close to each other, with similar consistency observed across different concentrations (Fig. S6, ESI[†]).

The polymer contribution to the complex modulus $|G^*|$ was measured using both DWS and DLS microrheology for the 0.5 wt% SDS solution, and results are compared in Fig. 4b. The upper frequency limit of DLS microrheology, approximately 10^4 rad s^{-1} (for $\theta = 90^\circ$), is lower than that of DWS. This reflects the higher resolution of the mean-square

displacement in DWS based on multiple scattering, compared to DLS based on simple scattering.

In Fig. 4b, while the trends in $|G^*|$ are similar for both DLS and DWS, the curves do not overlap. We found that, upon vertically shifting the DLS microrheology data by a factor of 3, the curves align well (open circles for shifted DLS data and filled squares for DWS data in Fig. 4b). The ratio $|G^*|_{\text{DWS}}/|G^*|_{\text{DLS}}$ remains reasonably constant within the overlapping frequency range (10^2 – 10^4 rad s $^{-1}$), with $|G^*|_{\text{DWS}}/|G^*|_{\text{DLS}} \approx 3$ (the inset of Fig. 4b). This indicates that the frequency dependences of $|G^*|_{\text{DWS}}$ and $|G^*|_{\text{DLS}}$ are consistent while their absolute value are different.

The discrepancy between $|G^*|_{\text{DWS}}$ and $|G^*|_{\text{DLS}}$ remains unexplained. We can speculate that this discrepancy may arise from interference between scattered light signals originating from both the probe particles and the micelles in the sample. Ideally, microrheological measurements detect only the light scattered by the probe particles, with the corresponding correlation function calculated accordingly. However, in practice, the light scattered by the surrounding viscoelastic medium may also be detected, leading to a mixing of the signals that distorts the autocorrelation function and reduces the accuracy of measurements. While DWS microrheology can mitigate this issue by operating at high probe particle concentrations, DLS microrheology, typically performed at low probe concentrations to avoid multiple scattering, faces greater challenges in isolating scattering from the probe particles. In this study, we attempted to reduce the influence of scattering from the wormlike micelles by increasing the probe concentration up to the multiple scattering limit; however, it might not be sufficient to fully eliminate the interference. Further systematic investigation is required to validate the applicability of DLS microrheology.

3.3.2 Analysis of bending and Zimm modes. DWS and DLS microrheology were successfully used to observe the bending and Zimm modes in the SDS/Al(NO $_3$) $_3$ aqueous solutions within the high-frequency regime.

According to classical theory of polymer dynamics, a solution of semiflexible chains under the bending and Zimm modes exhibits scaling behavior in the complex modulus:^{1,15}

$$|G^*(\omega)| \approx \begin{cases} c_n k_B T (\tau_0 \omega)^{1/3\nu} & (\omega < \tau_0^{-1}, \text{ Zimm mode}) \\ c_n k_B T (\tau_0 \omega)^{3/4} & (\omega > \tau_0^{-1}, \text{ bending mode}) \end{cases} \quad (5)$$

where c_n is the number density of the Kuhn monomer, and ν is the Flory exponent (0.588 for good solvents and 0.5 for θ solvents). The relaxation time of the Kuhn monomer, τ_0 , can be determined at the boundary between these two modes.

Fig. 5a shows the polymer contribution to $|G^*|$ derived from the DWS and DLS microrheological measurements for the representative SDS concentrations (0.5, 1, and 6 wt%). Data for other concentrations are shown in Fig. S7 (ESI †). The Zimm and bending modes are identified by their respective power-law exponents, 5/9 and 3/4, which are consistent with the theoretical prediction in eqn (5) (5/9 (= 0.56) corresponds to $1/3 \nu$ (= 0.57) for a good solvent with $\nu = 0.588$).^{1,37,38}

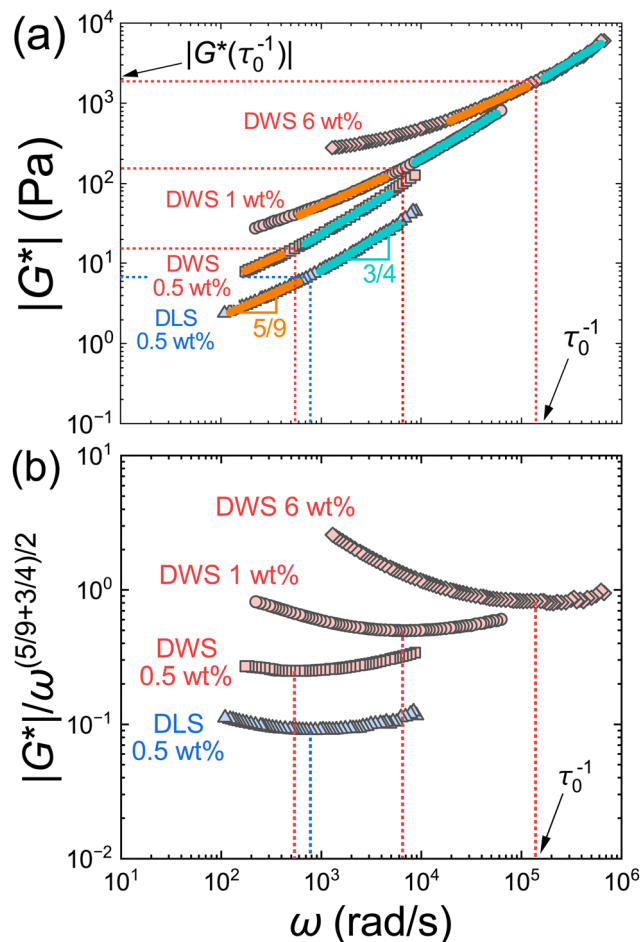


Fig. 5 (a) Polymer contribution to complex modulus of the 0.5, 1, and 6 wt% SDS solutions obtained by DWS and DLS microrheology (red and blue symbols). The lines show power-law behaviors with exponents of 5/9 (orange solid lines) and 3/4 (blue solid lines), corresponding to the Zimm and bending modes, respectively. (b) Value of $|G^*(\omega)|/\omega^{(5/9+3/4)/2}$ used to determine the crossover points between the two scaling laws.

In this study, the boundary between the two modes was identified from the local minimum of $|G^*(\omega)|/\omega^{(5/9+3/4)/2}$, where the exponent is the intermediate value between the scaling exponents of the Zimm (5/9) and bending (3/4) modes (Fig. 5b).^{15,39} From this boundary, the relaxation time of Kuhn monomers τ_0 and the corresponding modulus $|G^*(\tau_0^{-1})|$ were determined. While τ_0 has been extensively studied for various wormlike micellar systems and semiflexible polymers, the modulus $|G^*(\tau_0^{-1})|$ has received limited attention in the literature.¹⁵

3.3.3 Characteristic length and chain rigidity. The relaxation time of the Kuhn monomer (or the Zimm relaxation time), τ_0 , determines the Kuhn length b , which is calculated as $b = (k_B T \tau_0 / \eta_s)^{1/3}$, where η_s is the solvent viscosity.¹ Fig. 6 shows that the value of b decreases with increasing C_{SDS} (closed symbols). This behavior is commonly observed in wormlike micellar solutions of charged surfactants. As the surfactant concentration increases, charge screening by counterions reduces the repulsive forces between ionic micellar head groups,

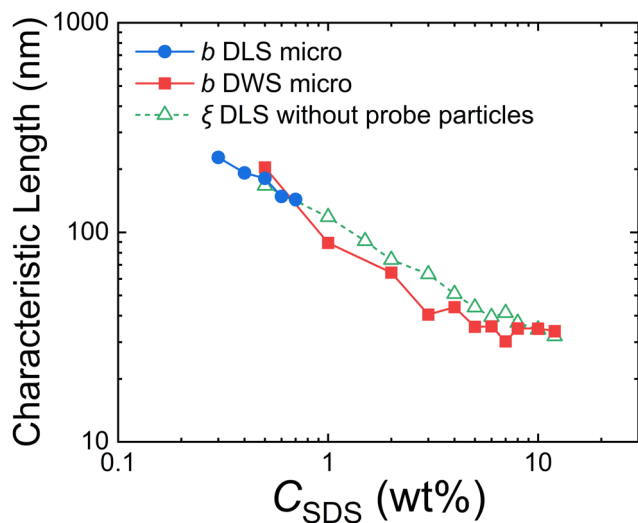


Fig. 6 Kuhn lengths b determined by DWS and DLS microrheology, and correlation length ξ determined by DLS (without probe particles) as functions of C_{SDS} .

thereby enhancing chain flexibility and decreasing the length scale over which the chains exhibit bending, b .^{12,13,40–44} At concentrations higher than about 5 wt%, the value of b becomes constant, indicating that the charge screening effect on the Kuhn length is inversely proportional to ionic strength and reaches an asymptote (approximately 30 nm) at sufficiently high concentrations.^{12,13,40–43}

The absolute values of b obtained from DWS and DLS measurements show good agreement, suggesting that the difference between $|G^*|_{\text{DWS}}$ and $|G^*|_{\text{DLS}}$ (Fig. 4b) has little impact on the frequency dependence of G^* , enabling the determination of τ_0 with reasonable accuracy (Fig. 5). Thus, both DWS and DLS microrheology are available for determining τ_0 and b .

The correlation length ξ , obtained from DLS without probe particles, is replotted in Fig. 6 (open triangles). The correlation length, which represents the intermolecular distance, decreases with increasing C_{SDS} , reflecting the denser entanglements, increased branching, and reduction in the Kuhn length b . In conventional flexible polymer systems, ξ is significantly larger than b (≤ 1 nm).¹ However, in this system, ξ and b are comparable due to the high rigidity of the chains, with b exceeding 10 nm. This indicates that each rigid correlation blob contains approximately one Kuhn monomer in this system.

3.3.4 Characteristic volume and monomer radius. The complex modulus at the relaxation time of the Kuhn monomer, $|G^*(\tau_0^{-1})|$, provides the characteristic volume of the Kuhn monomer $(1/c_n)_0$ as

$$\left(\frac{1}{c_n}\right)_0 \approx \frac{k_B T}{|G^*(\tau_0^{-1})|} \quad (6)$$

as derived from eqn (5).^{1,15} Within this characteristic volume, one Kuhn monomer is found. Fig. 7 plots $(1/c_n)_0$ (closed symbols) as a function of C_{SDS} . It decreases with increasing

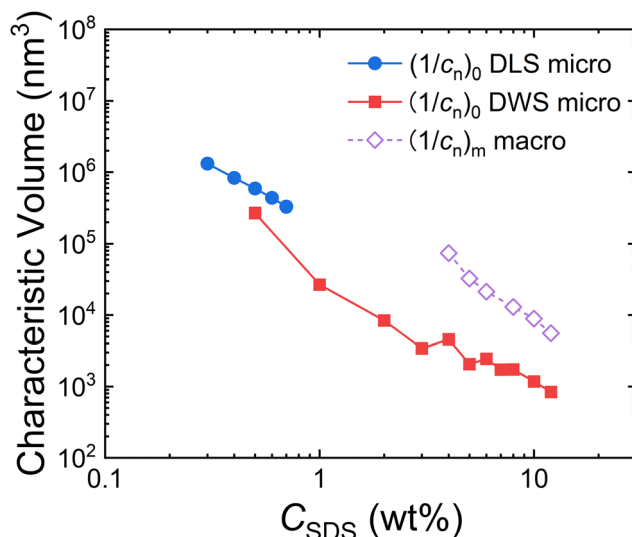


Fig. 7 Characteristic volume of Kuhn monomers determined by DWS and DLS microrheology, and mesh volume determined by macrorheology as functions of C_{SDS} .

C_{SDS} , consistent with the observed reduction in the Kuhn length. Even after the Kuhn length no longer decreases ($C_{\text{SDS}} > 5$ wt%), $(1/c_n)_0$ continues to decrease, reflecting further concentration of the Kuhn monomers (or the surfactants).

The $(1/c_n)_0$ values determined by DWS microrheology and DLS microrheology exhibit similar trends, while the absolute values show difference, reflecting the differences in $|G^*|$ (as shown in Fig. 4b), from which $(1/c_n)_0$ is derived.

To reveal hierarchical structure of the network, the larger characteristic volume, or mesh volume, is considered here. The mesh volume $(1/c_n)_m$ is conventionally determined by macrorheology using the plateau modulus G_e as $(1/c_n)_m \approx k_B T / G_e$.^{10,15,45} The values of $(1/c_n)_m$ shown in Fig. 7 (open diamonds) decrease with increasing C_{SDS} , reflecting denser entanglements and branching. Each mesh volume contains approximately 10 Kuhn monomers, as indicated by the ratio $(1/c_n)_m / (1/c_n)_0 = 7$ –16.

From the characteristic volume, $(1/c_n)_0$, the radius of the Kuhn monomer can be estimated. The volume $(1/c_n)_0$ contains a single Kuhn monomer at the same volume fraction as the entire system, ϕ ($\approx 0.01 C_{\text{SDS}}$).¹⁵ The cylindrical Kuhn monomer has the volume of $v_0 \approx \pi r^2 b$ (r is the cylinder radius), and its volume fraction is given by $\phi \approx v_0 (1/c_n)_0^{-1}$. Thus, the characteristic volume can be written as

$$\left(\frac{1}{c_n}\right)_0 \approx \frac{\pi r^2 b}{\phi} \quad (7)$$

and the radius of the Kuhn monomer is calculated as $r \approx \sqrt{(\phi/\pi b)(1/c_n)_0}$. Calculated r values are plotted as a function of C_{SDS} in Fig. 8. The resulting average radii are $r = 1.1 \pm 0.4$ nm from DWS microrheology and $r = 2.3 \pm 0.1$ nm from DLS microrheology. These values are consistent with reported radii of SDS wormlike micelles with various salts, ranging from 1.2 to 1.9 nm, which remain constant at identical salt concentrations

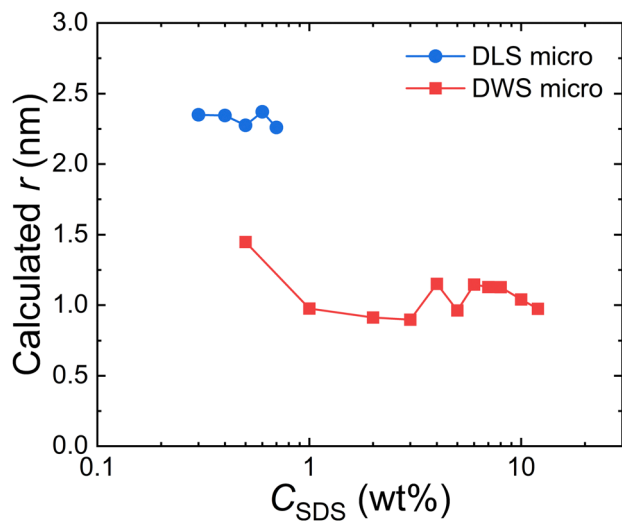


Fig. 8 Radius of the Kuhn monomers calculated from $(1/c_n)_0$.

due to the local packing of SDS molecules being independent of SDS concentration.^{7,8}

3.3.5 Characteristic volume and chain rigidity. The rigidity of the chains is also reflected in the characteristic volume $(1/c_n)_0$. Fig. 9a shows $(1/c_n)_0$ (closed symbols) as a function of C_{SDS} again, alongside the reference volume b^3 (open circles), for DWS and DLS microrheology. Across the studied concentration range, $(1/c_n)_0 < b^3$, indicating that the distance between neighboring Kuhn monomers is shorter than the Kuhn length. This suggests that $(1/c_n)_0$ contains both a Kuhn monomer and surrounding solvent, forming a space-filling structure in which adjacent volumes interact and repel each other with forces on the order of $k_B T$. Therefore, in this system, $(1/c_n)_0$ represents the correlation volume that includes one Kuhn monomer and its surrounding solvent, which supports the result in Section 3.3.3 ($\xi \approx b$). This relationship between Kuhn monomers and correlation blobs is characteristic of semiflexible wormlike micellar solutions with relatively long Kuhn lengths.¹⁵ In contrast, in flexible polymer solutions, b is much shorter than ξ , making the correlation volume the smallest space-filling characteristic volume.¹

The concentration regime boundaries in solutions of highly rigid chains are discussed in relation to the excluded volume.⁴⁶ The excluded volume of rigid monomers can be approximated as $2rb^2$,^{1,46} and this excluded volume aligns closely with $(1/c_n)_0$ in the current system (Fig. 9a). The boundary condition between semidilute and concentrated regimes for rigid chain solutions can be approximated as $(1/c_n)_0 \approx 2rb^2$, since intermolecular interactions remain negligible when $(1/c_n)_0 \gg 2rb^2$.⁴⁶ Given that $(1/c_n)_0 \approx 2rb^2$ across the studied conditions, the observed solutions can be considered to be in conditions between semidilute and concentrated solutions.

The axial ratio of the rigid Kuhn monomers also defines solution conditions. By substituting the boundary condition between semidilute and concentrated solutions, $(1/c_n)_0 \approx 2rb^2$, into eqn (7), the boundary condition for the volume fraction

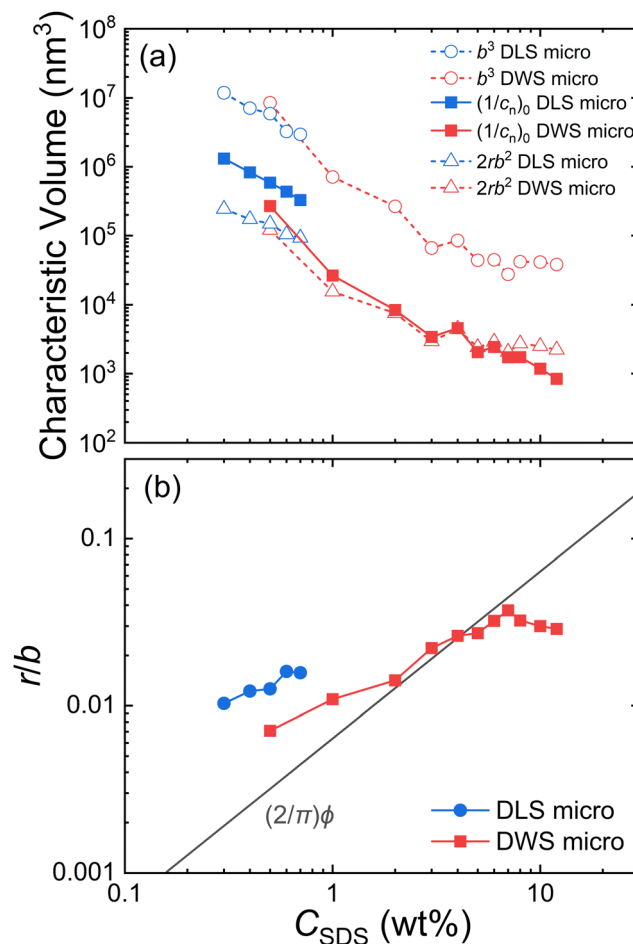


Fig. 9 (a) Characteristic volumes and (b) axial ratio of Kuhn monomers as functions of C_{SDS} .

can be expressed as

$$\phi \approx \frac{\pi r}{2b} \quad (8)$$

This relationship highlights that the axial ratio of Kuhn monomers, r/b , is a key parameter for characterizing solutions of semiflexible chains. As shown in Fig. 9b, r/b is comparable to $(2/\pi)\phi$ across the concentration regime, $C_{\text{SDS}} = 0.5$ to at least 7 wt%, suggesting that the solutions lie in the intermediate regime between semidilute and concentrated conditions. This behavior is attributed to the significantly small r/b ratio, which arises from the highly rigid structure of the Kuhn monomers with large b .

3.4 Molecular weight of Kuhn monomers

As demonstrated in our previous work,¹⁵ the molecular weight of unit segments at various hierarchical levels in polymer structures can be directly evaluated from their characteristic volume (or the inverse of their number density). Many unit segments in polymer systems exhibit a power-law relationship between the complex modulus and frequency.¹ Thus, macro- or micro-rheometry provide the characteristic volume based on the modulus at the relaxation time of the segments, as

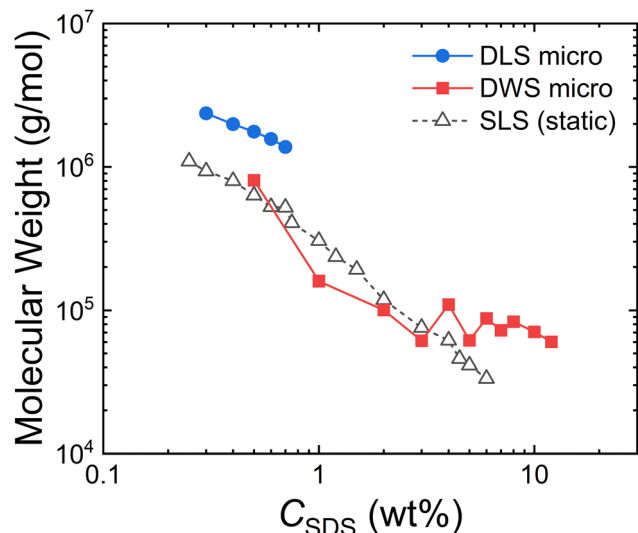


Fig. 10 Values of molecular weights of the Kuhn monomer determined by different methods as functions of C_{SDS} . DWS microrheology (M_0), DLS microrheology (M_0), and SLS (M_b).

described by eqn (6). Given the experimentally known density of polymer components, the weight per unit segment, or its molecular weight, can be calculated from the characteristic volume. For the bending and Zimm modes studied here, the molecular weight of the Kuhn monomer M_0 is determined from the space-filling characteristic volume $(1/c_n)_0$ obtained by DWS and DLS microrheology.¹⁵

$$M_0 = N_A c_w \left(\frac{1}{c_n} \right)_0 \quad (9)$$

where $c_w \approx 10 C_{\text{SDS}}$ is the weight concentration of SDS (C_{SDS} in wt%, and the mass density of the solution assumed to be 10^3 g L^{-1}).

Fig. 10 shows the values of M_0 determined by DWS microrheology and DLS microrheology, plotted as a function of C_{SDS} . The M_0 values, of the order of 10^4 – 10^6 g mol^{-1} , decrease with increasing C_{SDS} , consistent with the observed reduction in the Kuhn length until $C_{\text{SDS}} = 5 \text{ wt}\%$. Once the Kuhn length stabilizes ($C_{\text{SDS}} > 5 \text{ wt}\%$), M_0 does not change significantly, reflecting the fixed structure of the Kuhn monomers with the stable Kuhn length b and monomer radius r .

From SLS measurements, the molecular weight of the correlation blob M_b can be determined from the osmotic pressure as $\Pi \approx c_n k_B T \approx c_w N_A k_B T / M_b$ through Zimm plots (Fig. S8, ESI†).¹ The M_b values also decrease with increasing C_{SDS} and are comparable to the M_0 values obtained from microrheology, supporting the interpretation that each correlation blob contains a single Kuhn monomer. We were not able to accurately measure the molecular weight at the concentrations above 6 wt%, due to the slower components observed by DLS (Fig. 1a). Further static characterizations by small angle neutron scattering would be informative to argue the high concentration behaviors.

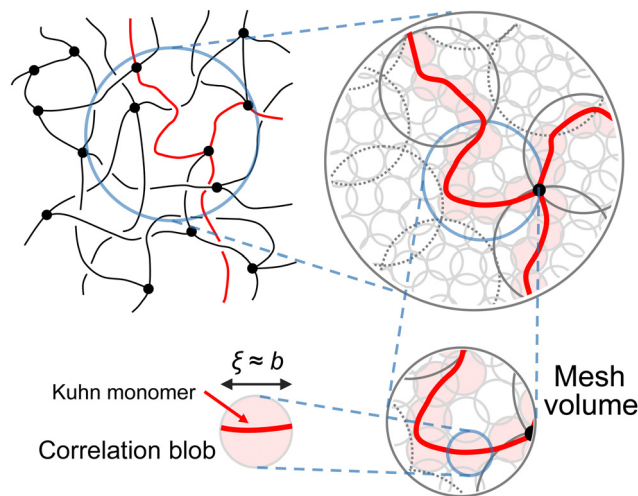


Fig. 11 Schematic illustrations of entangled and branched network structure of SDS wormlike micelles in this study.

3.5 Estimated structure of the wormlike micellar network

Integrating the results from the dynamic experimental methods used in this study, including DLS without probe particles, microrheology, and DWS and DLS microrheology, the network structure of the SDS wormlike micelles was estimated. A summary of the estimated structure has been presented in Fig. 11. The network structure forms following the linear-to-branched transition at approximately $C_{\text{SDS}} = 6 \text{ wt}\%$. The network consists of three- or four-point junctions and entanglement points.⁴ Each mesh (or network strand) contains approximately 10 correlation blobs or Kuhn monomers. Each correlation blob contains a single Kuhn monomer, a characteristic feature of semiflexible networks with high rigidity. Notably, in this system, the correlation volume, the characteristic volume of the Kuhn monomers (the volume in which one Kuhn monomer is found), and the excluded volume of the Kuhn monomers are comparable. The Kuhn monomer has the small axial ratio r/b , with the radius $r \approx 1 \text{ nm}$ and the large Kuhn length $b > 10 \text{ nm}$. The small r/b values arise from the small radius of the dodecyl chain in SDS and the large Kuhn length presumably due to high bending modulus. Aluminum ions are supposed to efficiently bind to three anionic SDS head groups, thereby increasing the bending modulus.

Importantly, this structural insight has been obtained not only by using the correlation length ξ , widely determined by DLS (without probe particles), but also by measuring the absolute value of the complex modulus $|G^*|$ through macro- and micro-rheometry. This structural characterization approach using $|G^*|$, which has not been extensively emphasized in previous studies, can be a powerful tool complementary to classical static methods.

4 Conclusion

The semiflexible network of SDS in the aqueous solution with $\text{Al}(\text{NO}_3)_3$ salt was characterized by the dynamic techniques. The

relaxation times of the fast and slow modes, along with the correlation length, were evaluated using DLS. Macrorheology provided the relaxation time of the slow mode, zero-shear viscosity, plateau modulus, and mesh volume. Using the relaxation times and absolute values of the complex viscoelastic moduli at the Zimm-bending boundaries, DWS and DLS microrheology offered the Kuhn length (or the persistence length), characteristic volume, radius, and molecular weight of Kuhn monomers, which align well with the results from the SLS measurements. Integrating insights from these characteristic parameters enables the estimation of the network structure composed of the mesh, correlation blobs, and Kuhn monomers. The demonstrated approach is theoretically applicable to various semiflexible polymer networks beyond wormlike micellar systems.

Data availability

Data for this article are available at Zenodo at <https://doi.org/10.5281/zenodo.15113705>.

Conflicts of interest

There are no conflicts to declare.

Acknowledgements

This work was supported by Mazume Research Encouragement Prize in Kyoto University and JSPS KAKENHI Grant Number JP23KJ1326.

Notes and references

- M. Rubinstein and R. H. Colby, *Polymer Physics*, Oxford University Press, New York, 1979.
- C. P. Broedersz and F. C. MacKintosh, *Rev. Mod. Phys.*, 2014, **86**, 995–1036.
- A. H. Clark and S. B. Ross-Murphy, *Adv. Polym. Sci.*, 1987, **83**, 57–192.
- J. Rothstein, *Rheol. Rev.*, 2008, **6**, 1–46.
- P. G. de Gennes, *Scaling Concepts in Polymer Physics*, Cornell University Press, New York, 2003.
- B. Chu and B. S. Hsiao, *Chem. Rev.*, 2001, **101**, 1727–1761.
- L. J. Magid, Z. Li and P. D. Butler, *Langmuir*, 2000, **16**, 10028–10036.
- L. Arleth, M. Bergström and J. S. Pedersen, *Langmuir*, 2002, **18**, 5343–5353.
- W. H. Tuminello, *Polym. Eng. Sci.*, 1986, **26**, 1339–1347.
- D. Calvet, J. Y. Wong and S. Giasson, *Macromolecules*, 2004, **37**, 7762–7771.
- N. Willenbacher, C. Oelschlaeger, M. Schopferer, P. Fischer, F. Cardinaux and F. Scheffold, *Phys. Rev. Lett.*, 2007, **99**, 068302.
- J. Galvan-Miyoshi, J. Delgado and R. Castillo, *Eur. Phys. J. E: Soft Matter Biol. Phys.*, 2008, **26**, 369–377.
- C. Oelschlaeger, M. Schopferer, F. Scheffold and N. Willenbacher, *Langmuir*, 2009, **25**, 716–723.
- C. Oelschlaeger, M. Cota Pinto Coelho and N. Willenbacher, *Biomacromolecules*, 2013, **14**, 3689–3696.
- H. Degaki, L. Jørgensen, T. Koga and T. Narita, *Macromolecules*, 2025, **58**, 314–320.
- M. Yada, M. Machida and T. Kijima, *Chem. Commun.*, 1996, 769–770.
- M. Yada, H. Hiyoshi, K. Ohe, M. Machida and T. Kijima, *Inorg. Chem.*, 1997, **36**, 5565–5569.
- D. Angelescu, A. Khan and H. Caldararu, *Langmuir*, 2003, **19**, 9155–9161.
- D. Angelescu, H. Caldararu and A. Khan, *Colloids Surf., A*, 2004, **245**, 49–60.
- D. Gu and F. Schüth, *Chem. Soc. Rev.*, 2014, **43**, 313–344.
- T. G. Mason and D. A. Weitz, *Phys. Rev. Lett.*, 1995, **74**, 1250–1253.
- D. A. Weitz and D. J. Pine, in *Dynamic Light Scattering: The Method and Some Applications*, ed. W. Brown, Oxford University Press, New York, 1993, pp. 652–720.
- M. Bellour, M. Skouri, J. P. Munch and P. Hébraud, *Eur. Phys. J. E: Soft Matter Biol. Phys.*, 2002, **8**, 431–436.
- T. G. Mason, K. Ganesan, J. H. van Zanten, D. Wirtz and S. C. Kuo, *Phys. Rev. Lett.*, 1997, **79**, 3282–3285.
- T. Tumolo, L. Angnes and M. S. Baptista, *Anal. Biochem.*, 2004, **333**, 273–279.
- B. R. Dasgupta, S.-Y. Tee, J. C. Crocker, B. J. Frisken and D. A. Weitz, *Phys. Rev. E: Stat., Nonlinear, Soft Matter Phys.*, 2002, **65**, 051505.
- W. Brown, K. Johansson and M. Almgren, *J. Phys. Chem.*, 1989, **93**, 5888–5894.
- E. Buhler, J. P. Munch and S. J. Candau, *J. Phys. II*, 1995, **5**, 765–787.
- N. Nemoto, M. Kuwahara, M.-L. Yao and K. Osaki, *Langmuir*, 1995, **11**, 30–36.
- S. Rose, A. Marcellan, D. Hourdet and T. Narita, *Macromolecules*, 2013, **46**, 5329–5336.
- M. E. Cates and S. J. Candau, *J. Phys.: Condens. Matter*, 1990, **2**, 6869.
- T. Shimada, M. Doi and K. Okano, *J. Chem. Phys.*, 1988, **88**, 2815–2821.
- T. J. Drye and M. E. Cates, *J. Chem. Phys.*, 1992, **96**, 1367–1375.
- I. A. Kadoma, C. Ylitalo and J. W. van Egmond, *Rheol. Acta*, 1997, **36**, 1–12.
- J.-F. Berret, in *Molecular Gels: Materials with Self-Assembled Fibrillar Networks*, ed. R. G. Weiss and P. Terech, Springer, Netherlands, 2005.
- N. Willenbacher and C. Oelschlaeger, *Curr. Opin. Colloid Interface Sci.*, 2007, **12**, 43–49.
- F. Gittes and F. C. MacKintosh, *Phys. Rev. E: Stat. Phys., Plasmas, Fluids, Relat. Interdiscip. Top.*, 1998, **58**, R1241–R1244.
- D. C. Morse, *Macromolecules*, 1998, **31**, 7030–7043.
- M. Tassieri, J. Ramírez, N. C. Karayiannis, S. K. Sukumaran and Y. Masubuchi, *Macromolecules*, 2018, **51**, 5505–5568.

- 40 L. J. Magid, Z. Han, Z. Li and P. D. Butler, *J. Phys. Chem. B*, 2000, **104**, 6717–6727.
- 41 C. Sommer, J. S. Pedersen, S. U. Egelhaaf, L. Cannavacciuolo, J. Kohlbrecher and P. Schurtenberger, *Langmuir*, 2002, **18**, 2495–2505.
- 42 L. Cannavacciuolo, J. S. Pedersen and P. Schurtenberger, *Langmuir*, 2002, **18**, 2922–2932.
- 43 B. A. Schubert, E. W. Kaler and N. J. Wagner, *Langmuir*, 2003, **19**, 4079–4089.
- 44 F. Nettesheim and N. J. Wagner, *Langmuir*, 2007, **23**, 5267–5269.
- 45 Some studies have estimated the mesh length ξ_m from the plateau modulus (or mesh volume) as $\xi_m \cong (Ak_B T/G_e)^{1/3}$, where A is a prefactor that changes depending on the system (See: W. Zou and R. G. Larson, *J. Rheol.*, 2014, **58**, 681–721; R. F. López-Santiago, J. Delgado and R. Castillo, *J. Colloid Interface Sci.*, 2022, **626**, 1015–1027). This study focuses on the mesh volume $(1/c_n)_m$, which can be directly obtained from G_e , rather than ξ_m , whose prefactor may vary depending on the system.
- 46 M. Doi and S. F. Edwards, *The Theory of Polymer Dynamics*, Oxford University Press, Oxford, 1986.